Incorporation of time-of-flight information reduces metal artifacts in simultaneous positron emission tomography/magnetic resonance imaging: a simulation study

Davison, Helen ; Ter Voert, Edwin E G W ; de Galiza Barbosa, Felipe ; Veit-Haibach, Patrick ; Delso, Gaspar

Abstract: OBJECTIVES: This study aimed to describe and evaluate the influence of time-of-flight (TOF) information on metal artifact reduction in positron emission tomography (PET) image quality in clinical simultaneous PET/magnetic resonance (MR) scanning. MATERIALS AND METHODS: A total of 7 patients with various malignant tumors were included and underwent a PET/MR examination after standard PET/computed tomography. Baseline TOF and non-TOF PET images were reconstructed. Next, the TOF and non-TOF PET reconstructions were repeated after the introduction of artificial signal voids in the attenuation map to simulate metal artifacts of various sizes in a range of locations. Three different sizes of signal voids were inserted in the attenuation maps for each location of interest: over the maxilla, humeral head, chest, sternum, thoracic and lumbar spine, as well as the femoral head to replicate clinically relevant metal artifacts. The reconstructed images with the artifacts were then compared with the baseline reconstructed images. The mean percentage error in a region of interest surrounding the simulated artifact was used to compare between TOF and non-TOF images. Further comparison between TOF and non-TOF images was performed using histogram analysis. RESULTS: In all cases, the mean percentage error in a region of interest surrounding the simulated artifact was reduced when TOF information was included in the reconstruction. The inclusion of TOF also changes the distribution of smaller errors away from the origin of the artifact. In some anatomical regions, an increase in the number of small errors was noted with TOF, although the differences with non-TOF were minimal. CONCLUSIONS: Positron emission tomographic imaging benefits from the integration of TOF information in simultaneous PET/MR. The inclusion of TOF information in simultaneous PET/MR imaging reduces errors related to metal artifacts at the site of the artifact.

DOI: https://doi.org/10.1097/RLI.0000000000000146

Incorporation of Time-of-Flight Information Reduces Metal Artifacts in Simultaneous Positron Emission Tomography/Magnetic Resonance Imaging
A Simulation Study

Helen Davison, BSc,† Edwin E.G.W. ter Voert, MSc,* Felipe de Galiza Barbosa, MD,*‡ Patrick Veit-Haibach, MD,*‡ and Gaspar Delso, PhD§*

Objectives: This study aimed to describe and evaluate the influence of time-of-flight (TOF) information on metal artifact reduction in positron emission tomography (PET) image quality in clinical simultaneous PET/magnetic resonance (MR) scanning.

Materials and Methods: A total of 7 patients with various malignant tumors were included and underwent a PET/MR examination after standard PET/computed tomography. Baseline TOF and non-TOF PET images were reconstructed. Next, the TOF and non-TOF PET reconstructions were repeated after the introduction of artificial signal voids in the attenuation map to simulate metal artifacts of various sizes in a range of locations. Three different sizes of signal voids were inserted in the attenuation maps for each location of interest: over the maxilla, humeral head, chest, sternum, thoracic and lumbar spine, as well as the femoral head to replicate clinically relevant metal artifacts. The reconstructed images with the artifacts were then compared with the baseline reconstructed images. The mean percentage error in a region of interest surrounding the simulated artifact was used to compare between TOF and non-TOF images. Further comparison between TOF and non-TOF images was performed using histogram analysis.

Results: In all cases, the mean percentage error in a region of interest surrounding the simulated artifact was reduced when TOF information was included in the reconstruction. The inclusion of TOF also changes the distribution of smaller errors away from the origin of the artifact. In some anatomical regions, an increase in the number of small errors was noted with TOF, although the differences with non-TOF were minimal.

Conclusions: Positron emission tomographic imaging benefits from the integration of TOF information in simultaneous PET/MR. The inclusion of TOF information in simultaneous PET/MR imaging reduces errors related to metal artifacts at the site of the artifact.

Key Words: artifacts, time-of-flight, PET/MR, image quality

(*Invest Radiol* 2015;00: 00–00)

The combination of positron emission tomography (PET) and magnetic resonance imaging (MRI) is a recent development in hybrid imaging. In hybrid PET/MRI, the anatomical information of MRI complements the functional and molecular information provided by PET.[1,2] In addition to its well-established advantages such as superior soft tissue contrast, MRI can also provide functional information, by using diffusion-weighted imaging, spectroscopy, and arterial spin labeling, among others. The prospect of combined functional information from PET and MRI means that there is an increasing interest into using PET/MRI for cardiology[3] and neurology[4] as well as its more obvious applications in oncology.[5]

Traditionally, PET is combined with computed x-ray tomography (CT) and the CT transmission data are used for PET photon attenuation correction. Computed tomographic images used for attenuation correction can be scaled to compensate for the higher-energy PET emission photons using a bilinear function.[6] However, magnetic resonance (MR) data cannot be used in the same way for PET/MRI attenuation correction because it is not related to the electron density of the tissue. Instead, MR data are related to the proton density and relaxation properties of the tissue; hence, it must be processed in a different way to approximate the PET photon attenuation.

Despite proposed methods for improving MR-based attenuation correction (MR-AC), such as template-based[7] and segmentation-based[8] methods, MR-AC for PET/MR remains challenging.[7–9] The associated problems with MR-AC are, among others, segmentation errors, inadequate tissue models (eg, where bone tissue is unaccounted for), and artifacts in the MR image caused by metal implants. These errors can cause inconsistencies in the MR-AC maps, causing lesions close to the implants to be obscured and resulting in incorrect assessment of the lesions.[9,10] Including time-of-flight (TOF) information in the PET image reconstruction algorithm has been shown to reduce these inconsistencies.[11,12] Inclusion of TOF information in PET/CT imaging has been shown to improve spatial resolution, signal-to-noise ratio, and lesion detectability.[12–18]

The clinical benefit of using TOF information to reduce the errors caused by metal artifacts can be applied to other hybrid PET imaging modalities. In PET/MRI, PET/CT, or any other hybrid imaging methods, the 2 imaging modalities should ideally yield complementary rather than redundant information. This means that the resultant hybrid imaging tool can be considered greater than the sum of its parts.[19–21] However, if either imaging modality has inferior quality or severe artifacts, the other imaging modality might be somewhat limited in recovering all information needed for correct diagnosis.

Recent developments in PET detector design have resulted in improved time resolution: a resolving time of less than 400 picoseconds, which gives a spatial uncertainty of less than 60 mm, is now achievable.[17] This improved time resolution means that TOF PET reconstruction is more robust because it is less sensitive to mismatched attenuation correction, erroneous normalization, and poorly estimated scatter correction. As the time resolution achievable with TOF improves, the reconstruction becomes more robust.[12]

Received for publication October 17, 2014; and accepted for publication, after revision, January 23, 2015.

From the *Department of Nuclear Medicine, University Hospital Zurich, University of Zurich, Zurich, Switzerland; †Department of Medical Physics, Royal United Hospitals Bath NHS Foundation Trust, Bath, United Kingdom; ‡Department of Diagnostic and Interventional Radiology, University Hospital Zurich, Zurich, Switzerland; and §GE Healthcare, Waukesha, WI.

Conflicts of interest and source of funding: Author Veit-Haibach received investigator-initiated study grants from Bayer Healthcare, Siemens Healthcare, Roche Pharmaceuticals, and speaker's fees from GE Healthcare. Author Delso is an employee of GE Healthcare. For the remaining authors, none were declared.

Authors Veit-Haibach and Delso equally contributed to this article.

Supplemental digital contents are available for this article. Direct URL citations appear in the printed text and are provided in the HTML and PDF versions of this article on the journal's Web site (www.investigativeradiology.com)

Reprints: Edwin E.G.W. ter Voert, MSc, Department of Nuclear Medicine University Hospital Zurich Rämistrasse 100 CH-8091 Zurich Switzerland. E-mail: Edwin.terVoert@usz.ch.

ISSN: 0020-9996/15/0000–0000

In this work, we compare and quantitatively analyze the effects of using TOF-PET with conventional PET imaging for PET-MR data sets containing simulated artifacts in the attenuation maps.

MATERIALS AND METHODS

Patients

Between January and June 2014, a total of 7 patients (2 women, five men; median age, 53 years; age range, 29–80 years; body mass index range: 22.1–24.9) participated in this prospective study. All patients were referred clinically for PET/CT examinations for either staging or restaging/follow-up of various malignant tumors. All patients underwent an additional subsequent scan in a new simultaneous TOF PET/MR scanner. Exclusion criteria were contraindications to MRI, for example, MRI-incompatible implants and claustrophobia. This study was approved by the local institutional medical ethics committee and relevant government authorities. Signed informed consent was obtained from each patient before inclusion into this study.

PET/CT Imaging

All patients were administered with radiopharmaceutical tracer ^{18}F-fluorodeoxyglucose (^{18}F-FDG) and fasted for 6 hours before being injected. The administered dose was 3 MBq/kg for patients weighing less than 85 kg; otherwise, it was 3.5 MBq/kg. After a standardized uptake period of 60 minutes, the clinically indicated PET/CT scan was performed according to the relevant local protocols. A subsequent TOF PET/MR scan was performed immediately after the initial PET/CT scan.

Time-of-Flight PET/MRI

A GE Signa PET/MR hybrid whole-body scanner (GE Healthcare, Waukesha, WI), which was not CE marked and not approved by the Food and Drug Administration at the time of this study, was used for the TOF PET/MR acquisition. The scanner comprises a 3-T wide-bore MR system with an MR-compatible TOF PET detector ring installed between the body and gradient coils. The detector ring consists of 28 modules, each one containing 4 × 15 subblocks and covering roughly 64.5 × 250 mm^2. In each subblock, an array of 3 × 2 silicon photomultipliers is paired with an array of 4 × 3 LYSO ($Lu_{1.8}Y_{0.2}SiO_5(Ce)$) scintillator crystals, each measuring 3.95 × 5.3 × 25.0 mm^3. The PET transaxial and axial fields of view are 600 mm and 250 mm, respectively.

The transaxial spatial resolution is approximately 4.2 mm, and axial resolution is 5.7 mm. The best achievable resolving time of the TOF detector is less than 400 picoseconds.[17]

The PET/MR acquisition was performed after each patient had undergone the clinically indicated PET/CT; the time of the PET/MR scan postinjection depended on the PET/CT program. On average, the PET/MR started 100 ± 21 minutes (mean ± SD) after injection. The patients were positioned in supine position with their arms down. Before the acquisition of the PET data, a whole-body MR localizer scan was performed in the craniocaudal direction. Next, the 3-dimensional (3D) PET emission scan was planned and started. The default number of bed positions was 6, from the vertex of the skull to the midthighs, but adjustable for each specific patient size. The default acquisition time per bed position was 3 minutes.

During the acquisition of each PET station, a 3D dual-echo, spoiled gradient recalled echo sequence (LAVA-FLEX) was started for attenuation correction. The whole-body protocol also included a high-resolution LAVA-FLEX sequence, a T2-weighted fast-recovery fast spin-echo (FRFSE) sequence, and a dedicated T2-weighted fast-recovery fast spin-echo with fat saturation and respiratory triggering for thoracic imaging.

MR-Based Attenuation Correction

Using the dual-echo LAVA-FLEX sequence, in-phase and out-of-phase images were acquired and water-only and fat-only images were calculated automatically.[22,23] The sequence parameters were as follows: repetition time, 4.056 milliseconds; out-of-phase echo time, 1.116 milliseconds; in-phase echo time, 2.232 milliseconds; flip angle, 12 degrees; field of view (frequency x phase direction), 500 mm × 375 mm; and acquisition matrix, 256 × 128, 1 slab with 64 × 5.2-mm^2-thick axial slices, voxel size of 1.95 × 2.93 mm^2, and 1 average. The body coil was used for the attenuation correction sequence, and the total acquisition time per bed position was 18 seconds.

While planning the PET emission scan, the user is prompted to set the anatomical regions (head, thorax, abdomen, pelvis) of the scan; with MR-based attenuation correction, an atlas is used for the patient's head and neck region. For the other regions of the body, the air, lung, and continuous fat/water segmentation is used for MR-AC. In the final step, TOF PET data are used for truncation completion.[8,9]

TOF and Non-TOF PET Reconstructions

All PET images were reconstructed twice for each data set. For the conventional non-TOF PET images, VUE Point HD was used. VUE Point HD is based on a 3D ordered subsets expectation maximization iterative reconstruction algorithm. This method of reconstruction includes scatter, dead-time, random, attenuation, and normalization corrections as well as correcting for the detector response using SharpIR but ignores the TOF information.[24] VUE Point FX was used for reconstructing the TOF PET images. The PET images were reconstructed using 3 iterations and 28 subsets, with a 600-mm diameter field of view and a 256 × 256 image grid with 2.34 × 2.34 × 2.78-mm^3 voxels. The images were filtered in image space using an in-plane Gaussian convolution kernel with a full width at half maximum of 2.0 mm, followed by a "light" axial filter with a 3-slice kernel.

Simulating Artifacts

The effects of artifacts on PET/MR images were investigated by simulating clinically realistic metal artifacts for both non-TOF and TOF PET reconstructions. The artifacts were simulated by inserting signal voids into the MR-AC map using a MATLAB (The MathWorks Inc., Natick, MA) based tool for editing attenuation maps; this editor tool can be used from the scanner host computer to edit each MR-AC map before the non-TOF and TOF PET reconstructions are performed.

Signal voids were inserted in the attenuation maps over the maxilla, humeral head, chest, sternum, thoracic and lumbar spine, as well as the femoral head. These signal voids produced artifacts representative of clinical artifacts owing to dental implants, shoulder joint replacements, port implants, sternotomy wires, spondylodesis in the thoracic and lumbar spine, and hip joint replacements (Fig. 1).

An elliptical volume with air-equivalent density was inserted into each low-resolution MR-AC map corresponding to the relevant anatomical region before reconstruction to produce a simplified model of an attenuation map containing clinical metal artifacts (See Supplementary Figure 1, Supplemental Digital Content 1, which shows examples of the modified attenuation maps, http://links.lww.com/RLI/A196). This modified attenuation map was used to reconstruct the data set twice: once with TOF information and once without. The modified MR-AC map was then edited again to simulate larger artifacts; each region was reconstructed to show the effects of 3 sizes of artifact (Table 1). The signal voids inserted into the attenuation maps to simulate dental implants, port implants, sternotomy wires, and metal orthopedic implants over thoracic spine and lumbar spine had transaxial diameters of 4.7 mm, 23.4 mm, and 51.6 mm. The diameters of the signal voids were chosen so that the artifacts were representative of the sizes of real clinical artifacts. Typically, hip and shoulder joint replacements cause larger artifacts; hence, signal voids with larger transaxial diameters (42.2 mm, 60.9 mm, 79.7 mm) were used to simulate these artifacts (Table 1).

FIGURE 1. An example of a coronal CT maximum intensity projection image showing clinical implants that would lead to artifacts in a PET reconstruction. This example shows a patient with dental implants, a port implant, surgical implants in the left humerus, a left hand ring, and a joint replacement in the left hip.

A further patient dataset was included and reconstructed, in order to show the improved lesion detectability in a region containing a metal artifact. Signal voids with transaxial diameters of 4.7 mm, 23.4 mm and 51.6 mm were inserted in the attenuation map close to a lesion in the maxilla for this data set.

Image Analysis

Each reconstructed artifact image was compared with the corresponding baseline image without artifacts for both TOF and non-TOF reconstructions.

A MATLAB program was applied to normalize the data sets to give a percentage deviation from baseline. This was performed by subtracting the baseline image from the image reconstructed with a simulated artifact for each artifact size and anatomical region and dividing these difference images again by the baseline image and multiplying it by 100. A mask was applied to remove regions outside the body and regions with low activity (<0.2 kBq/mL) because the relative error can be dominated by noise in these regions of low activity.

This normalized error was visualized using MATLAB, producing a contour map of the absolute percentage error over the image area that can be viewed simultaneously with the baseline PET image.

The mean absolute percentage error over a volume of interest (VOI), with a size of $10 \times 10 \times 10$ voxels, over the location of each signal void was calculated and compared for the TOF and non-TOF reconstructions for the maxilla, chest, sternum, and spinal regions. A larger VOI ($30 \times 30 \times 30$ voxels) was used to determine the mean absolute percentage error for the shoulder and hip regions.

For each artifact size (small, medium, and large), the mean absolute percentage errors in the TOF and non-TOF PET images were compared for each anatomical region using the Wilcoxon matched-pairs signed rank test (Prism 5.04; GraphPad Software Inc, San Diego, CA). *P* values less than 0.05 were considered statistically significant.

The percentage reduction in mean error magnitude when TOF information is included was calculated by comparing the mean absolute error values over the VOIs for each anatomical region. The corresponding error on each percentage reduction value was calculated from the standard deviations on the mean error values over the TOF and non-TOF VOIs.

Histogram analysis was performed on the TOF and non-TOF images to compare the voxel values in the images with artifacts to the baseline images. The percentage difference between the artifact image and the baseline image was calculated independently for each reconstruction; the errors are plotted to show the difference between TOF and non-TOF reconstructions for each anatomical region and artifact size. The frequency of the errors is plotted using a logarithmic scale so that the nonlinear incidence of errors in each reconstruction may be visualized.

The mean absolute error difference between TOF and non-TOF away from the induced signal void was also investigated. Therefore, a hollow 3D shell volume was defined around the artifact. The inner diameters were initially set to the signal void size, and outer diameters were 1 voxel larger. Next, the inner and outer diameters were (at the same time) stepwise increased by 1 voxel. For every step, the mean absolute error of all the voxels inside this shell volume that were also still in the patient's body area was calculated. The mean absolute errors for both the TOF and non-TOF reconstructed images were then plotted against the distance away from the artifact.

RESULTS

The Effect of TOF Information on Error Magnitude

In all 7 anatomical regions, the inclusion of TOF information into the reconstruction reduced the magnitude of the error caused by the artifact over the artifact location (Fig. 2, Table 2, and Supplementary

TABLE 1. Simulated Signal Void Location and Size

		Diameters (Transaxial/Axial) of Signal Voids, mm		
Location	**Artifact**	**Small**	**Medium**	**Large**
Maxilla	Dental implants	4.7/2.8	23.4/13.9	51.6/30.6
Humeral head	Shoulder joint replacement	42.2/25.0	60.9/36.1	79.7/47.3
Chest	Port implant	4.7/2.8	23.4/13.9	51.6/30.6
Sternum	Sternotomy wires	4.7/2.8	23.4/13.9	51.6/30.6
Thoracic spine	Spondylodesis	4.7/2.8	23.4/13.9	51.6/30.6
Lumbar spine	Spondylodesis	4.7/2.8	23.4/13.9	51.6/30.6
Femoral head	Hip joint replacement	42.2/126.6	60.9/182.8	79.7/239.1

Shoulder and hip joint replacements cause large clinical artifacts; hence, larger elliptical signal voids were used to simulate these effects.

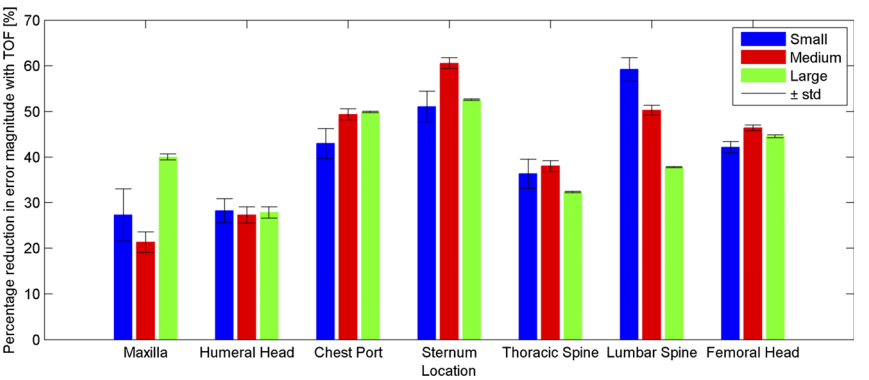

FIGURE 2. The percentage reduction in error magnitude when TOF information is included, plotted for each anatomical region. Two 30 × 30 × 30-voxel VOIs were used to analyze the effects of artifacts located near the femoral head and humeral head; all other anatomical regions were evaluated using 10 × 10 × 10-voxel VOIs. The percentage reduction in error is plotted for the 3 sizes of artifact (small, medium, and large) used for each anatomical region. The error bars show the propagation of error (standard deviation) on each mean error measurement when calculated as a percentage difference. Figure 2 can be viewed online in color at www.investigativeradiology.com.

Figures 2–8, Supplemental Digital Content 2, showing contour plots illustrating the absolute error in the maxilla, humeral head, chest port, sternum, thoracic spine, lumbar spine, and femoral head, respectively, http://links.lww.com/RLI/A195). For all artifact sizes (small, medium, large), the inclusion of TOF information significantly reduced the error caused by the artifact ($P < 0.02$, Wilcoxon matched-pairs signed rank test).

The most significant reductions in error magnitude were observed for artifacts simulated in the chest, sternum, and pelvic regions, where the errors were reduced by at least 40% using TOF (Figs. 2 and 3, Supplementary Figures 4, 5, and 8, Supplemental Digital Content 2, contour plots illustrating significant error reduction over chest, sternum and femoral head, respectively, http://links.lww.com/RLI/A195). For the pelvic region, the reductions are similar for each size of artifact; this similarity is also observed for the artifacts simulated in the humeral head (Fig. 2, Supplementary Figures 3 and 8, Supplemental Digital Content 2, which are figures that show the similarity in error reduction in the humeral head and femoral head, http://links.lww.com/RLI/A195).

TABLE 2. The Mean Absolute Percentage Error and Standard Deviation, Measured Over a Volume of Interest Positioned Over the Artifact Location, for Each Location and Artifact Size

Artifact Site	Transaxial Diameter of Signal Void, mm	Mean Absolute Percentage Error ± SD Over VOI		Error Reduction ± SD due to TOF, %
		Non-TOF	TOF	
Maxilla	4.7	0.4 ± 1.7	0.3 ± 1.3	27.3 ± 5.7
	23.4	13.4 ± 24.4	10.5 ± 17.9	21.3 ± 2.3
	51.6	66.6 ± 34.4	40.0 ± 24.4	40.0 ± 0.7
Humeral head	42.2	10.6 ± 21.5	7.6 ± 16.6	28.2 ± 2.6
	60.9	21.8 ± 30.8	15.8 ± 21.8	27.3 ± 1.8
	79.7	34.4 ± 34.7	24.9 ± 22.7	27.8 ± 1.2
Chest-port implant	4.7	0.8 ± 2.1	0.5 ± 1.4	43.0 ± 3.3
	23.4	34.2 ± 32.2	17.3 ± 19.2	49.4 ± 1.2
	51.6	92.4 ± 9.7	46.3 ± 7.4	49.9 ± 0.1
Sternum	4.7	0.7 ± 1.9	0.3 ± 1.0	51.1 ± 3.3
	23.4	33.3 ± 31.4	13.1 ± 14.4	60.5 ± 1.2
	51.6	93.4 ± 9.1	44.3 ± 10.0	52.6 ± 0.2
Thoracic spine	4.7	0.9 ± 2.3	0.6 ± 1.6	36.3 ± 3.2
	23.4	36.5 ± 34.1	22.6 ± 24.8	38.0 ± 1.2
	51.6	93.4 ± 9.7	63.2 ± 10.6	32.3 ± 0.16
Lumbar spine	4.7	1.1 ± 2.3	0.5 ± 1.2	59.2 ± 2.6
	23.4	40.9 ± 34.1	20.3 ± 22.0	50.3 ± 1.1
	51.6	96.8 ± 5.9	60.3 ± 11.5	37.8 ± 0.1
Femoral head	42.2	32.1 ± 31.1	18.6 ± 20.8	42.1 ± 1.2
	60.9	63.8 ± 31.4	34.2 ± 20.7	46.4 ± 0.6
	79.7	86.4 ± 19.2	47.9 ± 14.7	44.6 ± 0.3

All values were measured over a 10 × 10 × 10-voxel VOI, apart from the errors measured in the femoral head and humeral head, where a 30 × 30 × 30-voxel VOI was used.

TOF indicates time of flight; VOI, volume of interest.

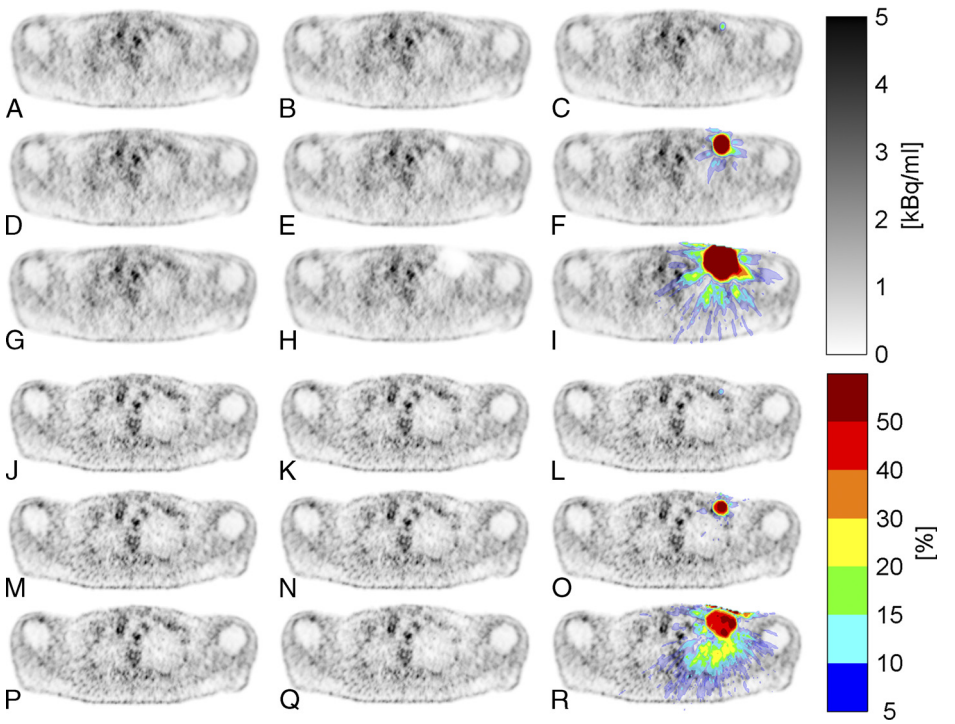

FIGURE 3. Axial PET images showing the effect of 3 sizes of simulated artifact on non-TOF images (A–I) and TOF images (J–R) for the chest, with a signal void inserted in a typical clinical location for a port implant. The color map shows discrete contours representing percentage errors from 5% to 10% to higher than 50%. A, D, G, J, M, and P, The baseline PET images, reconstructed with no artifacts. B and K, The PET images reconstructed with 4.7-mm transaxial diameter signal voids. E and N, The 23.4-mm transaxial diameter signal voids. H and Q, The 51.6-mm transaxial diameter signal voids (Table 1). C, F, I, L, O, and R, The images B, E, H, K, N, and Q overlaid with the corresponding error contour are shown, respectively. Figure 3 can be viewed online in color at www.investigativeradiology.com.

Artifacts simulated in the maxilla had the smallest reduction in error magnitude; the error measured over the medium artifact was reduced by 21% when the image was reconstructed using TOF (Fig. 2, Supplementary Figure 2, Supplemental Digital Content 2, http://links.lww.com/RLI/A195).

Histogram Analysis of TOF and Non-TOF Errors

The histograms of the normalized errors (Fig. 4, Supplementary Figures 9–14, Supplemental Digital Content 3, http://links.lww.com/RLI/A197) show an asymmetrical peak around zero, with a certain number of positive errors of magnitude less than 50% in most cases and negative errors that range up to −100%. Many of the higher positive (>25%) errors originate from relative low-signal areas. The signal void created in the attenuation map results in a lower activity signal in the same region in the reconstructed PET image. This causes the large negative error tail in the histograms. The histograms generated for artifacts simulated in the maxilla, chest port, sternum, as well as thoracic and lumbar spine show similar trends for TOF and non-TOF errors for each size of artifact (Fig. 4, Supplementary Figures 9, 11–13, Supplemental Digital Content 3, http://links.lww.com/RLI/A197). For the small and medium artifact sizes, the TOF reconstructions of these anatomical locations show a lower count for the negative errors compared with the non-TOF errors. In the large artifacts, the TOF reconstructions show a higher count for the lower negative errors (range, −5% to −20%),

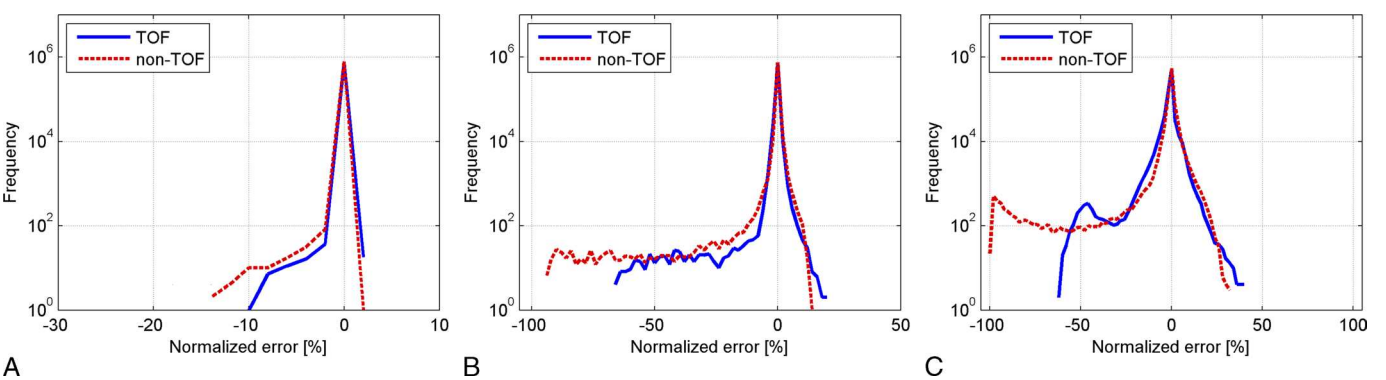

FIGURE 4. Histograms showing the frequency of normalized error when comparing artifact images with the baseline image for TOF (solid blue line) and non-TOF (dashed red line) reconstructions. A, B, and C, The difference from baseline for small, medium, and large artifacts (Table 1) inserted into the chest to simulate a port implant. The data were analyzed using a bin size of 2%, and error frequency is plotted logarithmically. Figure 4 can be viewed online in color at www.investigativeradiology.com.

whereas the non-TOF reconstructions show a higher count for the higher negative errors (range, −50% to −100%). For example, Figure 4C shows that TOF has more voxels with lower negative errors (range, −5% to −20%) than non-TOF. This can be interpreted together with the corresponding contour plot of Figure 3R. There, the TOF reconstruction shows errors in the range of −5% to −20% in regions away from the central artifact area where, in contrast, the non-TOF reconstruction shows lower errors (Fig. 3I). The voxels in and around the artifact area, on the other hand, have much higher error values in non-TOF (Fig. 3I) compared with TOF (Fig. 3R). This effect can also be seen in the histogram (Fig. 4C) where large numbers of non-TOF voxels with a high negative error (−50% up to −100%) have a lower negative error (between −20% and −50%) in TOF.

Histogram analyses of errors over the humeral head and femoral head (Supplementary Figures 10 and 14, Supplemental Digital Content 3, http://links.lww.com/RLI/A197) show a wider histogram curve in these cases than for the other anatomical regions. These histograms do show a pattern similar to other anatomical regions, with more small-magnitude negative TOF errors (up to −60%) for bigger artifacts and a greater number of larger-magnitude (−60% to −100%) non-TOF errors for all sizes of artifact.

The mean absolute error in regions away from the induced signal void was comparable for TOF and non-TOF in all 7 anatomical regions (Supplementary Figure 15, Supplemental Digital Content 3, http://links.lww.com/RLI/A197).

The Effect of TOF on a Lesion Near an Artifact

In the patient case where a metal artifact was simulated close to a lesion in the maxilla, the effect of the artifact on the lesion can be assessed, with and without TOF reconstruction. The clinical benefit of the artifact reduction is shown because the anterior extent of the tumor can be better appreciated in the TOF reconstruction than in the non-TOF image (Supplementary Figure 16, Supplemental Digital Content 3, http://links.lww.com/RLI/A197).

DISCUSSION

To our knowledge, this is one of the first studies that quantitatively evaluate the influence of TOF information in simultaneous PET/MR image data sets containing simplified models of clinically relevant metal artifacts. In all cases, the incorporation of TOF information into the reconstruction reduced the impact of artifacts on the reconstructed PET/MR image. The smallest percentage error reduction with TOF was 21% for the medium-sized artifact in the maxilla, and the largest percentage error reduction with TOF was 60% for the medium-sized artifact in the sternum. The magnitudes of the errors caused by artifacts simulated in the chest, sternum, and pelvic regions were reduced by more than 40% in the region around the origin of the artifact when TOF reconstruction was applied.

The similar reduction in magnitude between artifact sizes and the comparable histogram curves observed for the pelvic and shoulder regions is attributed to the fact that these regions had larger simulated artifacts than the other anatomical regions.

Although the contour plots and VOI analysis show this reduction in error over the artifact location in each anatomical region, the impact on the image as a whole is not so clear-cut. The histogram comparison between TOF and non-TOF reconstructions indicates that there is an increase in the number of small magnitude errors owing to simulated metal artifacts occurring in TOF-reconstructed images compared with the non-TOF reconstructed images. From the contour plots, it follows that the inclusion of TOF changes the distribution of smaller errors away from the origin of the artifact. In some anatomical regions, an increase in the number of small errors was noted with TOF, although the mean differences with non-TOF are minimal. The non-TOF reconstructed images, on the other hand, show larger central artifact regions and can have large error spots in the region near the artifact.

Reconstruction of PET images using TOF information is less sensitive to data inconsistencies such as inaccurate attenuation correction than PET reconstruction without TOF.[12] This is also evident from comparison of PET reconstructions of regions using VOI analysis (Fig. 2) and has also been reported in clinical cases by dual board-certified radiologists/nuclear medicine physicians.[11]

It has recently been shown that redundant TOF information reduces cross-talk artifacts when attempting to reconstruct the activity and attenuation images simultaneously.[25,26] The capability of TOF to reduce attenuation correction errors is expected to become better as TOF timing resolution improves.[27]

On a side note, previous studies have shown the difference in the effects of dental artifacts on TOF and non-TOF PET images to be minimal; this was attributed to the use of the head atlas during reconstruction.[11] In the current study, the attenuation map was modified after the application of the head atlas to simulate an artifact. The femoral head artifact could also be different in real patient cases because the current reconstruction software does not allow air voids inside the body for the pelvic bed position. The model, however, gives a good estimate of the impact of the artifact in TOF- and non-TOF–reconstructed PET images, for example, for situations where the signal void extends to the air outside of the body.

The benefit of using TOF information is most obvious for large artifacts caused by metal implants, but it can also be applied to other attenuation inconsistencies, for example, due to patient motion or truncated attenuation maps.[12,28]

There are also MR techniques available to correct for metal artifacts. By correcting the metal artifacts in the MR image, the PET image will also be improved, regardless of whether TOF reconstruction is used. Several techniques including MAVRIC and short echo time imaging are already available for PET/MR and have shown their potential in metal artifact correction.[29,30] Incorporating TOF information in PET reconstructions alongside these techniques will possibly reduce the impact of metal artifacts on PET/MR images still further.

The limitation of our study is that only 7 patients were included; a larger patient population would improve the statistical power of the study. If a larger patient population was used for the study, patient body mass index could then be used to group the patients into underweight, healthy, and overweight subgroups to assess the effect of patient size on the artifact related errors. Using different MRI techniques with TOF PET to correct for metal artifacts and further reduce the artifact-related errors in PET/MR would be an interesting area for future investigation.

CONCLUSIONS

Positron emission tomography imaging benefits from the integration of TOF information in simultaneous TOF PET/MR. The inclusion of TOF information in simultaneous PET/MRI reduces errors related to metal artifacts at the site of the artifact.

REFERENCES

1. Disselhorst JA, Bezrukov I, Kolb A, et al. Principles of PET/MR imaging. *J Nucl Med*. 2014;55(suppl 2):2S–10S.
2. Nensa F, Beiderwellen K, Heusch P, et al. Clinical applications of PET/MR: current status and future perspectives. *Diagn Interv Radiol*. 2014;20:438–447.
3. Rischpler C, Nekolla SG, Dregely I, et al. Hybrid PET/MR imaging of the heart: potential, initial experiences, and future prospects. *J Nucl Med*. 2013;54:402–415.
4. Son Y-D, Cho Z-H, Choi E-J, et al. Individually differentiated serotonergic raphe nuclei measured with Brain PET/MR imaging. *Radiology*. 2014;272:131547.
5. Buchbender C, Heusner TA, Lauenstein TC, et al. Oncologic PET/MRI, Part 1: tumors of the brain, head and neck, chest, abdomen, and pelvis. *J Nucl Med*. 2012;53:928–938.

6. Burger C, Goerres G, Schoenes S, et al. PET attenuation coefficients from CT images: experimental evaluation of the transformation of CT into PET 511-keV attenuation coefficients. *Eur J Nucl Med Mol Imaging*. 2002;29:922–927.
7. Wollenweber SD, Ambwani S, Delso G, et al. Evaluation of an atlas-based PET head attenuation correction using PET/CT & MR patient data. *Nucl Sci*. 2013; 60:3383–3390.
8. Wollenweber SD, Ambwani S, Lonn AHR, et al. Comparison of 4-class and continuous fat/water methods for whole-body, MR-based PET attenuation correction. *Nucl Sci*. 2013;60:3391–3398.
9. Hofmann M, Pichler B, Scholkopf B, et al. Towards quantitative PET/MRI: a review of MR-based attenuation correction techniques. *Eur J Nucl Med Mol Imaging*. 2009;36(suppl 1):S93–S104.
10. Andersen FL, Ladefoged CN, Beyer T, et al. Combined PET/MR imaging in neurology: MR-based attenuation correction implies a strong spatial bias when ignoring bone. *Neuroimage*. 2014;84:206–216.
11. ter Voert E, Delso G, Ahn S, et al. *The Effect of TOF on PET Reconstructions in Patients With (Metal) Implants in Simultaneous TOF PET/MR Scanning*. Chicago, IL: Radiological Society of North America 2014 Scientific Assembly and Annual Meeting; 2014.
12. Conti M. Why is TOF PET reconstruction a more robust method in the presence of inconsistent data? *Phys Med Biol*. 2011;56:155–168.
13. Conti M. Focus on time-of-flight PET: the benefits of improved time resolution. *Eur J Nucl Med Mol Imaging*. 2011;38:1147–1157.
14. Surti S, Karp JS, Popescu LM, et al. Investigation of time-of-flight benefit for fully 3-D PET. *IEEE Trans Med Imaging*. 2006;25:529–538.
15. Surti S, Karp JS. Experimental evaluation of a simple lesion detection task with time-of-flight PET. *Phys Med Biol*. 2009;54:373–384.
16. Surti S. Update on time-of-flight PET Imaging. *J Nucl Med*. 2015;56:98–105.
17. Levin C, Glover G, Deller T, et al. Prototype time-of-flight PET ring integrated with a 3 T MRI system for simultaneous whole-body PET/MR imaging. *J Nucl Med*. 2013;54:148.
18. Lois C, Jakoby BW, Long MJ, et al. An assessment of the impact of incorporating time-of-flight information into clinical PET/CT imaging. *J Nucl Med*. 2010;51: 237–245.
19. Kuhn FP, Hüllner M, Mader CE, et al. Contrast-enhanced PET/MR imaging versus contrast-enhanced PET/CT in head and neck cancer: how much MR information is needed? *J Nucl Med*. 2014;55:551–558.
20. Reiner C, Stolzmann P, Husmann L, et al. Protocol requirements and diagnostic value of PET/MR imaging for liver metastasis detection. *Eur J Nucl Med Mol Imaging*. 2014;41:649–658.
21. von Schulthess GK, Veit-Haibach P. Workflow considerations in PET/MR imaging. *J Nucl Med*. 2014;55(suppl 2):19S–24S.
22. Bley TA, Wieben O, François CJ, et al. Fat and water magnetic resonance imaging. *J Magn Reson Imaging*. 2010;31:4–18.
23. Dixon WT. Simple proton spectroscopic imaging. *Radiology*. 1984;153:189–194.
24. Alessio AM, Stearns CW, Shan T, et al. Application and evaluation of a measured spatially variant system model for PET image reconstruction. *IEEE Trans Med Imaging*.2010;29:938–949.
25. Defrise M, Rezaei A, Nuyts J. Time-of-flight PET data determine the attenuation sinogram up to a constant. *Phys Med Biol*. 2012;57:885–899.
26. Rezaei A, Defrise M, Bal G, et al. Simultaneous reconstruction of activity and attenuation in time-of-flight PET. *IEEE Trans Med Imaging*. 2012;31:2224–2233.
27. Boellaard R, Hofman MB, Hoekstra OS, et al. Accurate PET/MR Quantification Using Time of Flight MLAA Image Reconstruction. *Mol Imaging Biol*. 2014;16:469–477.
28. Turkington TG, Wilson JM. Attenuation artifacts and time-of-flight PET. *Nuclear Science Symposium Conference Record (NSS/MIC), 2009 IEEE, Oct. 24, 2009–Nov. 1, 2009*. 2009;2997–2999.
29. Burger I, Gunzinger JM, Delso G, et al. *MR Artifact Reduction for Dental Alloys Using MAVRIC Sequences*. Milan, Italy: The International Society for Magnetic Resonance in Medicine, 2014.
30. Schramm G, Maus J, Hofheinz F, et al. Evaluation and automatic correction of metal-implant-induced artifacts in MR-based attenuation correction in whole-body PET/MR imaging. *Phys Med Biol*. 2014;59:2713–2736.